Applied Thermal Engineering 133 (2018) 493–500

Contents lists available at ScienceDirect

Applied Thermal Engineering

journal homepage: www.elsevier.com/locate/apthermeng

Research Paper

A three-dimensional model for thermoelectric generator and the influence of Peltier effect on the performance and heat transfer

Mingjian Liao[a,b,c], Zhu He[a,b,c,*], Chengpeng Jiang[a,b,c], Xi'an Fan[a,b,c,*], Yawei Li[a,b,c], Fengsheng Qi[d]

[a] The State Key Laboratory of Refractories and Metallurgy, Wuhan University of Science and Technology, Wuhan 430081, China
[b] National-provincial Joint Engineering Research Center of High Temperature Materials and Lining Technology, China
[c] Key Laboratory for Ferrous Metallurgy and Resources Utilization of Ministry of Education, Wuhan University of Science and Technology, Wuhan 430081, China
[d] School of Metallurgy, Northeastern University, Shenyang 110819, China

HIGHLIGHTS

- A 3-D model for thermoelectric modules which consisting of 127 thermocouples is developed.
- An experiment was carried out to validate the simulation.
- Influence of Peltier effect on the performance and heat transfer is investigated.
- The Peltier effects are proved to be more remarkable for weak heat transfer boundary conditions.

ARTICLE INFO

Keywords:
Thermoelectric generator
Peltier effect
Equivalent thermal conductivity
Output power
Efficiency

ABSTRACT

Thermoelectric generator has been considered as a promising device to recover industrial waste heat for electricity generating. To figure out the heat transfer and electric conduction processes in thermoelectric generator, a three-dimensional numerical model has been built up which consists of 127 thermocouples. The open-circuit voltage, internal resistance, and output power have been studied by numerical simulation. All calculation results are in good agreement with the experimental results, and the maximum deviation is less than 6%. Due to the influence of Peltier effect, both heat flow and equivalent thermal conductivity increases by 30.2% when temperature difference between the hot and cold side is 170 °C and the thermoelectric generator reaches its maximum power output. In addition, the Peltier effect has been investigated when the convective heat transfer boundary conditions are applied. The results showed that the effective temperature difference was raised to 13.6 °C (a 10.2% increase) and maximum output power was raised to 0.59 W (a 14.8% increase) for the thermoelectric generator model with a fin height of 100 mm when compared with that without fins. Besides that, the radio of load resistance to internal resistance decreased from 1.31 to 1.14.

1. Introduction

In recent years, thermoelectric generator (TEG) is attracting more and more attention due to its ability to generate electricity from waste heat [1,2]. TEG has many advantages, such as no moving parts, no chemical reaction, no pollution, no noise and a longer lifespan [3–5]. Moreover, as a solid-state heat engine, TEG generates a voltage whenever there is a temperature gradient. Therefore, TEG can be used to recover the energy in many processes in which heat is released directly to the atmosphere. Therefore, TEG is recognized as one of the most potential energy technologies in the 21st century [6].

Thermoelectric effects have been discovered for more than 40 years and many researchers have been concentrating on the investigations of improving the thermoelectric properties of materials [7,8]. In addition, optimizing the structure of thermoelectric devices based on thermal analysis is also an important way to improve the performances of TEG. Consequently, precise, complete description of the thermoelectric coupling process in the thermoelectric devices and analysis of the influence of various factors on the output index are vital for the amelioration of TEG's performance.

So far, computation tools have been used to build one-dimensional [9,10] or three-dimensional [11,12] heat transfer model, and the performances of TEG can be obtained by solving electric potential distribution and temperature distribution. More recently, Kossyvakis et al.

* Corresponding authors at: Department of Thermal Energy Engineering, School of Materials and Metallurgy, Wuhan University of Science and Technology, Wuhan 430081, China (Z. He). P.O. Box 185#, School of Materials and Metallurgy, Wuhan University of Science and Technology, 947 Heping Road, Qingshan District, Wuhan 430081, China (X. Fan).
E-mail addresses: hezhu@wust.edu.cn (Z. He), xafan@wust.edu.cn (X. Fan).

https://doi.org/10.1016/j.applthermaleng.2018.01.080
Received 14 September 2017; Received in revised form 15 December 2017; Accepted 21 January 2018

[13] investigated the temperature distribution on the hot side and performance reduction by thermal losses based on a finite element model which consists of 71 thermocouples. The discrepancy between computation and measurements is acceptable, which indicates that the model can be used in the evaluation of TEG's performances.

However, accurate prediction of the power production can be difficult because many heat transport mechanisms occur simultaneously in TEG. In early attempts, the numerical and experimental results were compared using single thermocouples [14,15]. It indicated that the temperature dependence properties of materials have a significant impact on calculation results and the contact thermal resistance should not be neglected [16]. In general, p-type and n-type thermoelectric material have the similar index called the figure of merit (ZT). So the p-type and n-type elements have the same geometric size and the devices can be assembled more conveniently. However, the similar ZT does not mean the same material properties such as the similar thermal conductivity and resistivity. So the p-type and n-type elements were treated as two separate parts and the differences in thermal behavior between the two elements are distinguished and evaluated [12]. Later, the influences of size effect on the power generation and thermal stresses were investigated based on a model which consists of two thermocouples. The results indicated that the power outputs and the efficiencies are related to the leg size and spacing [17]. More recently, Li et al. [18] pointed out that attention should be paid to the contact electrical resistance induced by welding. However, the studies mentioned above are limited to the investigation of single or a few thermocouples behaviors. In real situations, a commercial TEG module usually consists of a large number of thermocouples. Chen et al. [12] mentioned that the number of thermocouples has a significant impact on the TEG devices' cooling power. And they also [19] pointed out that the number of thermoelectric elements affects the power output and efficiency. Thus, a new holonomic model is needed for the full analysis of heat transfer and electric conduction processes in TEG.

As mentioned above, the computational method is a reliable tool to predict the performances and optimize the geometry structure of TEG. Besides, a precise and complete model must contain the following features: (1) the p-type and n-type must be treated as two separate parts and all the material properties are temperature-dependent; (2) the model must contain, besides P/N junction and conductive strips, a solder layer and ceramic plates; (3) the model should contain enough P/N junction if the computation conditions are allowed.

Moreover, there are still some difficulties in establishing a finite element model that couple with heat, electricity, and fluid flow at the same time. Thus, the following two methods are often used to calculate the output performance when TEG operating in fluids with temperature difference: (1) Firstly the liquid-solid conjugate heat transfer is calculated to determine the temperature field. Then the TEG's temperature of the hot and cold sides are used as the boundary condition for the calculation coupled with heat and electricity [18]; (2) Only the temperature field is calculated by simplifying the TEG model and the electric energy output is approximated by zero-dimensional model according to the obtained temperature field [20]. Both these two methods are based on the assumption that TEG is in an open-circuit state. However, when TEG is in a closed state, the Peltier effect produced by the current usually transfers extra dozens W of heat flow from the hot side [21]. The temperature field previously established may be changed significantly, especially when the heat transfer condition is weak such as the convective heat transfer with air. Under these conditions, the temperature difference between the two sides of TEG will be directly reduced and a relatively large deviation will appear in the final results. Nevertheless, there are few articles that discuss the extent of the influence of Peltier effect on different heat transfer conditions.

In this paper, a new complete TEG model consisting of 127 thermocouples has been developed and a laboratory TEG system has been built to verify the accuracy of the model. The open circuit voltage, internal resistance and maximum output power have been studied by numerical simulation and experiment. The p-type and n-type are treated as two separate parts and are based on temperature-dependent properties. In addition, the performance of TEG in a closed state, not in an open circuit state as previously done, has been investigated and the influences of Peltier effect on the performances, the temperature distribution and the equivalent thermal conductivity of the TEG under the convective heat transfer boundary conditions have been analyzed.

2. Theoretical model

TEGs' operation bases on the Seebeck effect: when two dissimilar conductors join together and form a closed loop, a voltage is produced due to a temperature difference between the two junctions. To obtain a greater voltage, a certain amount of thermoelement pellets are connected in series through copper strips and are sandwiched between two ceramic plates. The TEG module is connected to a load resistance to output electric energy during operation.

When the electric field and temperature field exist simultaneously, all processes occurring in the thermoelectric element can be expressed as:

$$\vec{j} = \frac{1}{\rho}(\vec{E} - \alpha\nabla T)$$

$$\vec{q} = \alpha T\vec{j} - \kappa\nabla T$$

where $\vec{E}$ is the electric field intensity; $\vec{j}$ is current density; $\vec{q}$ is heat flux; T is temperature; α, ρ, and κ are the Seebeck coefficient, electrical resistivity and thermal conductivity of a thermoelectric element, respectively.

An energy balance analysis for the p and n thermoelements leads to the energy equation [22]:

$$C_p a_p \frac{\partial T_p}{\partial t} = \nabla^2\kappa_p(x,y,z,T)\cdot T_p - jT_p\alpha_p(x,y,z,T) + j^2\rho_p(x,y,z,T)$$

$$C_n a_n \frac{\partial T_n}{\partial t} = \nabla^2\kappa_n(x,y,z,T)\cdot T_n + jT_n\alpha_n(x,y,z,T) + j^2\rho_n(x,y,z,T)$$

In which, subscripts p and n represent the materials p and n, respectively; C denotes the specific heat and a is density.

In steady state, the heat loss along the side of thermoelectric elements and Thomson effect are ignored. Taking into account the temperature dependence of material properties α, ρ, and κ, the steady-state heat transfer equation can be written as:

$$Ca\frac{\partial T}{\partial t} = 0 = \nabla^2\kappa(x,y,z,T)\cdot T - jT\alpha(x,y,z,T) + j^2\rho(x,y,z,T)$$

The electric potential equation can be written as [23]:

$$\nabla^2\phi(x,y,z) = -\alpha\nabla^2 T$$

where φ is the electric scalar potential.

3. Performance of TEG

The open circuit voltage (U_0) is calculated as [24,25]:

$$U_0 = n\cdot(\alpha_p + |\alpha_n|)\cdot(T_h - T_c)\cdot\left(\frac{R_i}{R_i + R_l}\right) = n\cdot\alpha_{pn}\Delta T\cdot\left(\frac{R_i}{R_i + R_l}\right)$$

where n is the number of thermocouples in TEG module; T_h is the temperature of hot side; T_c is the temperature of cold side; R_i is the thermal resistance of thermocouples; R_l is the total contact thermal resistance of TEG module.

The output power gets the maximum value (P_{max}) when the load resistance r_l value is equal to the internal resistance r_i:

$$m = \frac{r_l}{r_i} = 1$$

$$P_{\max} = \frac{(n\cdot\alpha_{pn}\cdot\Delta T\cdot R_i)^2}{4r_i\cdot(R_l + R_i)^2}$$

where m represents the ratio of the load resistance to the internal resistance, when m satisfies the following relationship:

$$m = \sqrt{1 + \frac{1}{2}Z(\overline{T}_h + \overline{T}_c)}$$

Maximum conversion efficiency (η_{max}) can be obtained:

$$\eta_{\max} = \frac{T_h - T_c}{T_h}\cdot\frac{m-1}{m + T_c/T_h}$$

where $\overline{T}_h$, $\overline{T}_c$ is the temperature of thermoelements' hot and cold side, respectively.

4. Numerical method

A three-dimensional finite element model of the TEG1-127-1.4-1.6 TEG module is built in the commercial software ANSYS AIM. The governing equations mentioned above are solved in association with the boundary conditions.

The dimensioning of the TEG module is 40 mm × 40 mm × 3.8 mm (width × depth × length). And the module is composed of 127 pairs of thermocouples and the size of semiconductor grain is 1.4 mm × 1.4 mm × 1.6 mm. Electrical connection is established through copper strips. The ceramic plates act as electric insulation and heat conduction. In addition, an external load resistor is electrically coupled with the electrodes of the TEG module in the present model.

The grid systems and geometric structures of TEG are displayed in Fig. 1. Four different grids with total elements of grid i = 100,984, grid ii = 34,820, grid iii = 17,779, grid iv = 9388 are tested and compared with each other to seek an appropriate grid system. In the four grid systems, the output power and conversion efficiency versus load resistance are calculated under the temperature of the hot side and cold side are 200 °C and 30 °C, respectively. The results show that the discrepancies among the curves of grid i, grid ii, grid iii are almost imperceptible. The maximum deviation between the results of grid ii and grid iii is less than 0.5%, while the results of grid iv differs greatly from others, which indicates that the grid iii system with 17,779 elements is proper for the simulation. Therefore, to save computation efforts without loss in accuracy, the grid iii is adapted.

The materials' temperature-dependent properties are listed in Table 1. Boundary conditions have been set as follows: the load resistor is electrically coupled with the electrodes of TEG. Constant temperature and convective heat transfer condition are applied directly to the TEG's hot and cold sides.

5. Experiments

To verify the accuracy of the TEG model, an experiment was set up. As shown in Fig. 2, the experiment system consists of a commercial TEG1-127-1.4-1.6 module, an aluminum plate heater, a recycled water cooling system, an adjustable load resistor and data acquisition system. The aluminum plate heater is controlled by a Proportion Integration Differentiation (PID) electrical system (accuracy, ± 1 °C) and a digital regulator. The recycled water cooling system is composed of a heat exchanger and a circulating constant temperature reservoir (accuracy, ± 0.1 °C). The aluminum plate of the heater is attached directly to the hot side of the TEG module, and its temperature is fixed at 40 °C, 50 °C, 60 °C, 100 °C, 140 °C, 180 °C and 220 °C, respectively. The recycled water cooling system is used to maintain the cold side

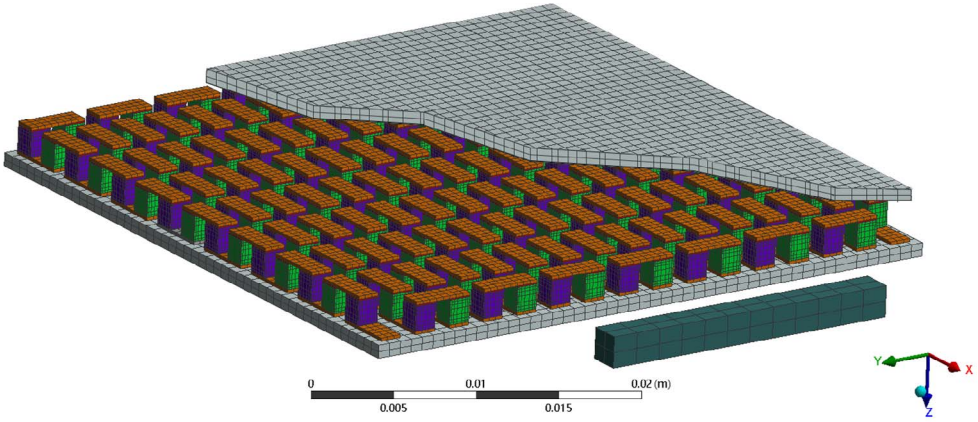

(c)

(a)

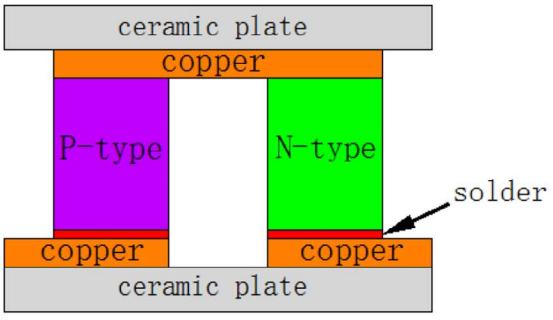

(b)

Fig. 1. (a) The geometric structures and grid systems of TEG; (b) the actual TEG module; (c) stacking structure of TEG module.

Table 1
The materials' properties.

Name	Thermal conductivity (W/m K)	Seebeck coefficient (μV/k)	Electric resistivity (10^{-5} Ω m)
Ceramic plate	22	–	–
Copper	385	–	1.78×10^{-3}
P-type	$4.8482^{-5} \times T^2$ $-0.0332 \times T$ $+6.949$	$-4.5312 \times 10^{-6} \times T^3$ $0.0012 \times T^2$ $0.8712 \times T$ -27.09	$-1.3348 \times 10^{-5} \times T^2$ $+0.01748 \times T$ -2.95643
N-type	$3.07 \times 10^{-5} \times T^2$ $-0.02031 \times T$ $+4.72174$	$-1.6797 \times 10^{-5} \times T^3$ $+0.02219 \times T^2$ $-9.356 \times T$ $+1054.78$	$-1.63839^{-5} \times T^2$ $+0.01681 \times T$ -2.61014
Solder	20	–	1.285

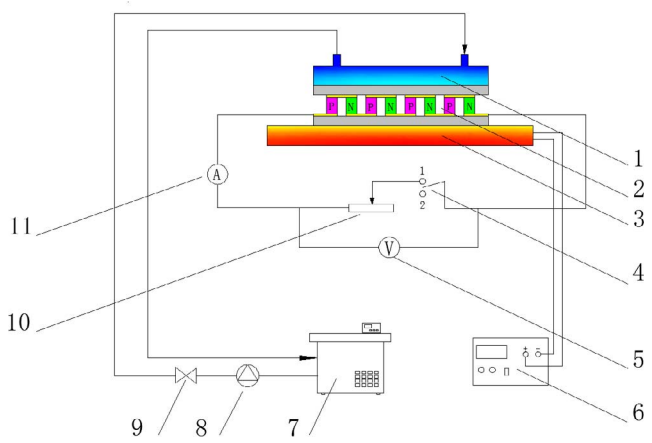

Fig. 2. Schematic illustration of the experimental setup of TEG. 1 – Cold side heat exchanger. 2 – TEG module. 3 – Aluminum plate heater. 4 – SPDT switch. 5 – Voltmeter. 6 – PID electrical system. 7 – Constant temperature reservoir. 8 – Pump. 9 – Valve. 10 – Variable resistor. 11 – Amperemeter.

temperature at 30 °C. To reduce contact thermal resistance and ensure that the two sides are heated evenly, both hot and cold side surfaces of the TEG module are coated with thermal grease. The voids between the heat and cold heat conducting components are filled with heat insulation material to reduce heat transfer between them and to improve the thermoelectric conversion efficiency. The clamping member was controlled by a pressure sensor, which provides the efficient pressure and prevents the module from excessive pressure damage.

When the temperature difference is constant and single-pole double-throw (SPDT) Switch is connected to point 2 (shown in Fig. 2), the voltmeter shows its open-circuit voltage (U_0); when the SPDT Switch turns to point 1 (shown in Fig. 2), the voltmeter shows the load voltage (U_L). The r_i of the TEG module is obtained using the matching load method and it can be calculated by [26]:

$$r_i = \frac{(U_0 - U_L)}{U_L} r_l$$

When $U_L = 1/2\ U_0$, $r_i = r_l$ and the value of r_i can be directly measured. The P_{max} is directly evaluated from the current and voltage measurements on r_l using the voltammetry method.

6. Results and discussion

The potential distributions when the hot side is 200 °C and the cold side is 30 °C are shown in Fig. 3(a). As can be seen, the direction of the potential growth is in line with the series of the thermoelements. The voltage across the load resistor is equal to TEG's positive and negative electrode voltages. Fig. 3(b) shows the temperature distributions for the corresponding conditions. As shown in Fig. 3(b), the internal temperature drop of the TEG model mainly occurs in the thermoelements.

Fig. 4 presents the measured and simulated open-circuit voltage, internal resistance and output power of the TEG. The test temperature range and the results deviation are present in Table 2. The open-circuit voltage and internal resistance curves present linear behavior, whereas the output power increases parabolically with the increase of the temperature gradient between the two sides of the generator. The maximum relative deviation is less than 6%, which indicates that the numerical results present very good agreement with the experimental results. The contact thermal resistance caused by the gap between the module and heat exchanger may be one of the reasons for the deviations.

The variations of the output power and conversion efficiency with load resistance, when the temperature of hot side is 200 °C and that of the cold side is 30 °C, are shown in Fig. 5. It can be seen that the output power and conversion efficiency increase initially and decrease afterward as the load resistance increases. The output power reached its maximum value (4.7 W) as the load resistance is 3.6 Ω, and the conversion efficiency reached the maximum value (4.5%) when the load resistance is 4.5 Ω. As shown in Fig. 4(b), the internal resistance value of TEG is 3.5 Ω when working in this same temperature range. For lithium batteries, it is generally known that the highest output power is

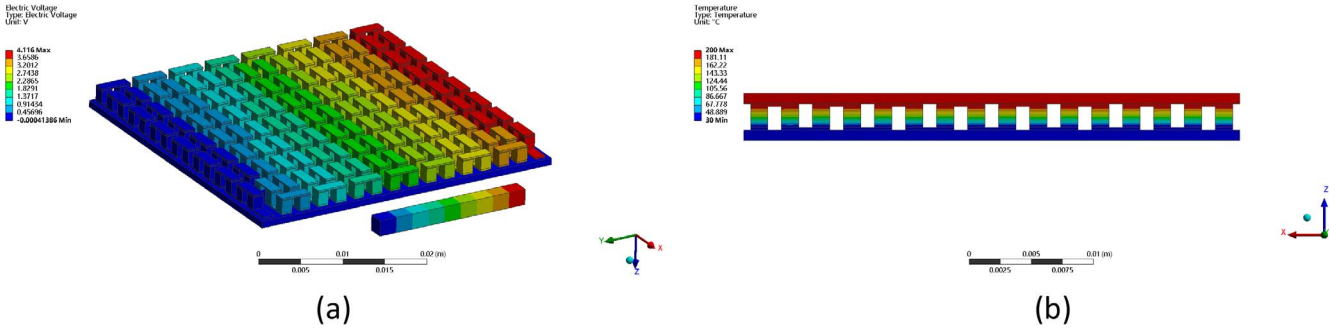

Fig. 3. Voltage contour (a) and temperature contour (b) for T_H = 200 °C and T_c = 30 °C.

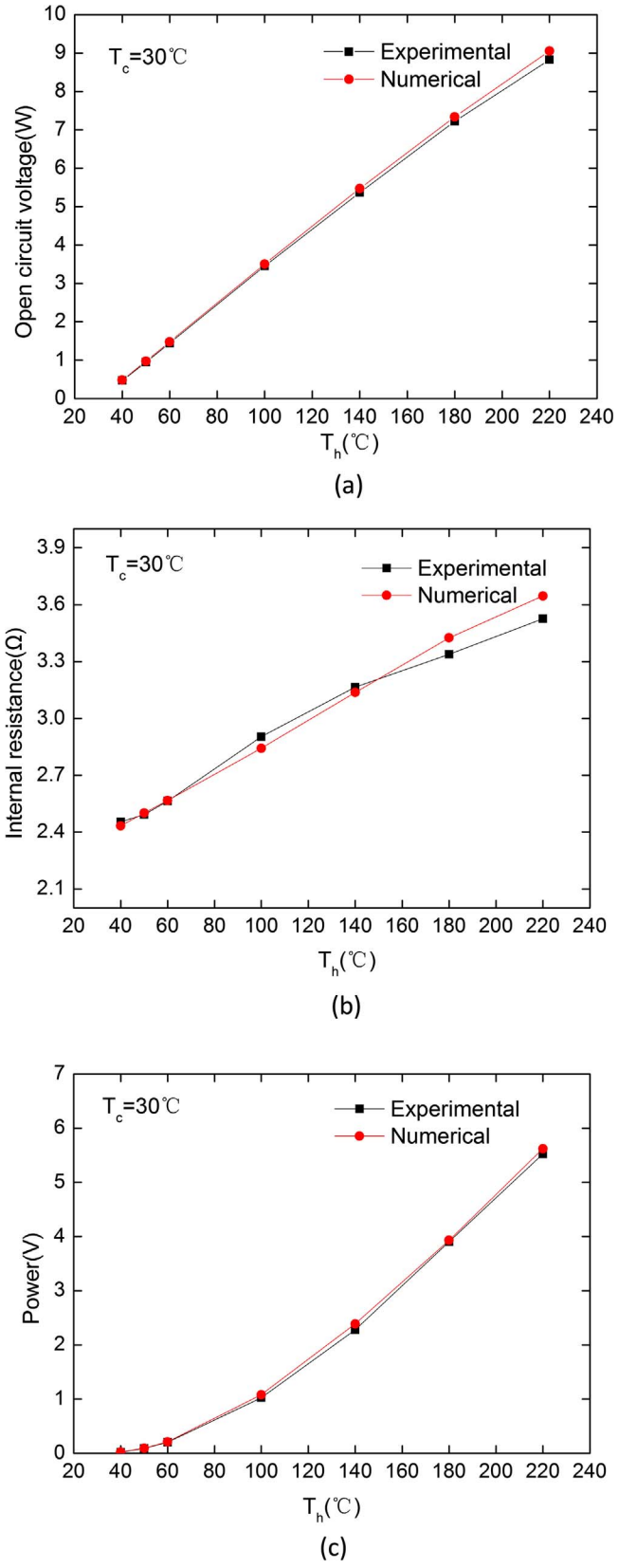

Fig. 4. Comparison between numerical and experimental performance curves-open circuit voltage (a), internal resistance (b), output power (c).

obtained when the load resistor is equal to the battery resistance, whereas the TEG does not comply with this rule. The inconsistency of the load and internal resistance when output power of TEG reaches the

Table 2
Comparison of open-circuit voltage, internal resistance and output power between computational model and experimental data.

Parameters	T_c (°C)	T_h (°C)	Deviation (%)
Open-circuit voltage, U_0 (V)	30	40–220	4.1
Internal resistance, R_i (Ω)	30	40–220	5.2
Output power, P (W)	30	40–220	5.8

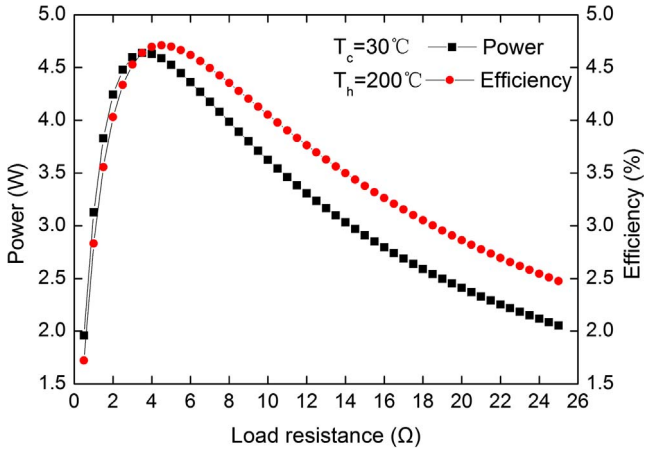

Fig. 5. The output power and efficiency variation with load resistance.

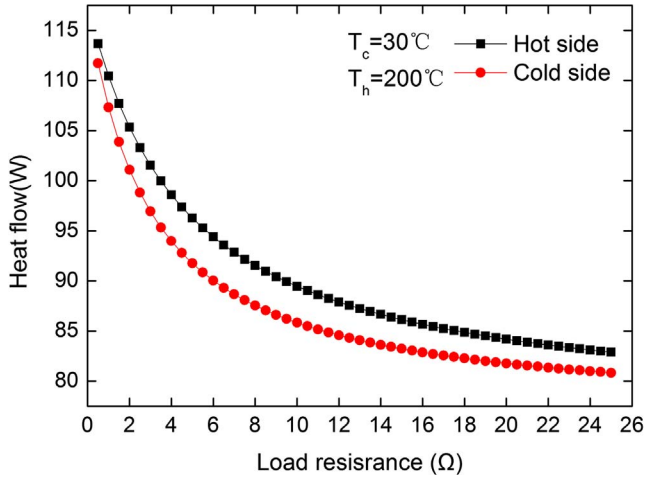

Fig. 6. The variation of heat flow of hot and cold sides with load resistance.

maximum is due to the Peltier effects produced by carrier transport, which increases the heat flow from the hot side to the cold side. Although the temperature of the TEG's cold and hot sides is kept constant, the additional heat flow makes the temperature difference between the ceramic plates and the semiconductor grains increase, which result in a reduction in the effective temperature difference of the TEG (the temperature difference between the hot end and the cold end of the thermoelements). Thus, increasing load resistance and decreasing current will lead to an increase in the voltage of TEG. Also, the output power increases correspondingly. Consequently, when output power of TEG reaches the maximum, the load resistance is greater than the internal resistance.

To study the influence of Peltier effects on heat transfer, the heat flow versus the load resistance is calculated in Fig. 6. It is showed that the heat flow cross the hot side to cold side decreases gradually and finally reaches a plateau period (76.6 W) when the load resistor increases. Because of the thermoelectric conversion, the heat flow at the hot and cold sides is inconsistent, and the difference of the heat flow

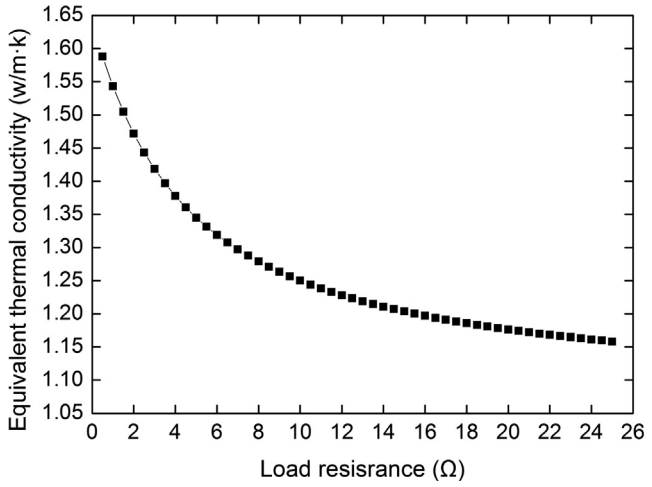

Fig. 7. The variation of equivalent thermal conductivity with load resistance.

between the hot and cold sides is the output power:

$$P = Q_h - Q_c = IU$$

where Q_h and Q_c is the heat flow through the hot and cold sides, and the conversion efficiency can be calculated by:

$$\eta = \frac{Q_h - Q_c}{Q_h} = \frac{P}{Q_h}$$

With the load resistance revised up to 3.6 Ω, the heat flow between the hot and cold sides reaches the maximum, and the maximum output power is achieved correspondingly. When the TEG is in open circuit, the heat flow through the hot and cold sides is $Q_h = Q_c = 76.6$ W. However, as shown in Fig. 6, the heat flow at the hot side is up to 99.7 W (a 30.2% increase) when the TEG reaches the maximum output power. According to the Fourier heat conduction law, the temperature difference between the hot side of ceramic plate and the hot side of the thermoelements should increase by 30.2% correspondingly. Similarly, the temperature difference between the cold side of the ceramic plate and the cold side of the thermoelements will also increase by 30.2%. However, from the calculation results, it is showed that the effective temperature difference decreases by just 2% than that in the open circuit due to the constant temperature boundary conditions. That is to say, the influence of the Peltier effects on the output performance is limited in such cases.

It is important to note that many researchers are usually interested in how TEGs are arranged on the heat source, hoping to provide a suitable temperature difference for TEG [27]. To do this, the TEG module is usually simplified to a stuffed bulk with an equivalent thermal conductivity depending on the heat flow [20]. The complex heat transfer process in the TEG module is approximated as heat conduction in the bulk, and the equivalent thermal conductivity is calculated by the law of Fourier heat conduction:

Table 3
The equivalent heat transfer coefficient and ambient temperature for each case.

	Equivalent heat transfer coefficient ($w/m^2 k$)	Ambient temperature (℃)
H_{fin1} = 0 mm	20	2593.3
H_{fin2} = 25 mm	169.3	482.8
H_{fin3} = 50 mm	296.3	361.6
H_{fin4} = 75 mm	390.4	322.6
H_{fin5} = 100 mm	453.5	305.5

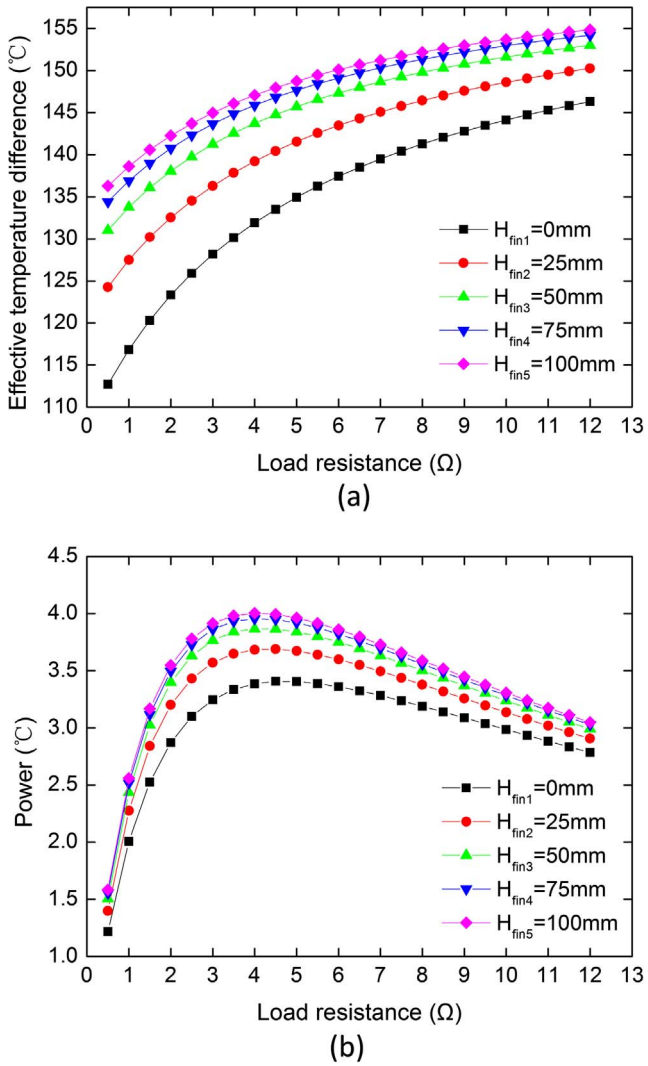

Fig. 9. The variation of heat flow of hot and cold side with load resistance (a); the variation of output power with load resistance (b).

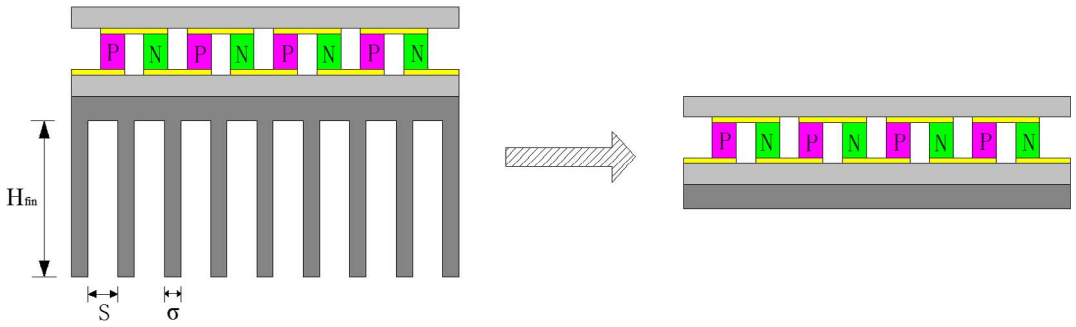

Fig. 8. The schematic of heat collector.

$$\lambda_{eff} = \frac{Q_h \cdot h}{\Delta T \cdot f}$$

However, there are at least two limitations with this simplified method. One is that the heat transfer in TEG module is anisotropic, which is usually neglected when calculating the equivalent thermal conductivity. The other, more importantly, because of the influence of the Peltier effect, the heat flow cross the module varies greatly with the current for the same temperature difference, which makes the equivalent thermal conductivity of the simplified model not approximated by that in the open circuit state. Fig. 7 shows that the equivalent thermal conductivity of TEG module versus the current. It can be seen that when the module reaches the maximum output power, the equivalent thermal conductivity is up to 1.393 $W/m^2 k$, increasing by 30.2% when compared with that in the open circuit state (1.070 $W/m^2 k$).

On the other hand, in real situations, the heat transfer conditions provided to TEG usually cannot keep the hot side at a constant temperature [28]. According to the previous analysis, it was found that the difference between the load resistance and the internal resistance is not very evident, when the heat transfer conditions on both sides of the TEG are good (temperature at the boundaries is constant). However, when the heat transfer conditions is weak (convective heat transfer conditions, just as in most real situations), the Peltier effect may have greater influence on the performance and heat transfer in these circumstances, and the ratio of load and internal resistance may significantly improve. To confirm this, the influence of Peltier effect on the temperature distribution and output performance of TEG under the different heat transfer intensity in the hot side was investigated.

The numerical model includes a TEG model and a fin heat collector. The fin heights H_{fin} are 10 mm, 25 mm, 50 mm, 75 mm and 100 mm, respectively. The fin heat collector is simplified by the method as that in the study of Meng et al. [29] (Fig. 8). To ensure that the equivalent and real heat collector have the same heat absorption, the equivalent heat transfer coefficient (h_{eff}) between the equivalent heat collector and the ambient is calculated by:

$$h_{eff} = h_f \cdot \frac{S + \frac{th\left(\sqrt{\frac{2h_f}{\lambda_{fin}\sigma}}\cdot\left(H_{fin}+\frac{\sigma}{2}\right)\right)}{\sqrt{\frac{2h_f}{\lambda_{fin}\sigma}}\cdot\left(H_{fin}+\frac{\sigma}{2}\right)}(2H_{fin}+\sigma)}{S+2H_{fin}+\sigma} \cdot \frac{S+2H_{fin}+\sigma}{S+\sigma}$$

where th is the hyperbolic tangent function, h_f is the convective heat transfer coefficient, and it is assumed to be 20 $W/(m^2\,°C)$, λ_{fin}, σ; S is the thermal conductivity, thickness and spacing of fins. In this work, λ_{fin} = 237 $w/(m^2\,°C)$, σ = 1.5 mm, S = 5 mm.

To ensure the temperature at hot side is 200 °C in open-circuit case, the ambient temperature is calculated by the Newton's law of cooling:

$$Q_h = (T_\infty - T_h) \cdot f \cdot h_{eff}$$

where T_∞ is the ambient temperature, f is the surface area of hot side. The h_{eff} and T_∞ versus H_{fin} are shown in Table 3. In the open-circuit state, the hot side temperature is 200 °C in all cases, which denotes a proper heat collector that can provide a suitable temperature difference for the TEG module with lower fluid temperature.

As shown in Fig. 9, the effective temperature difference between the hot side and cold side of the thermoelements, and the output power vary with the load resistance for different fin heights (H_{fin}) when the convective heat transfer condition is supplied. Owing to the influence of Peltier effects, the temperature at the hot side is reduced and the output power is lower than that of the previous case. At the same time, the increase of the load resistance reduces the current, which makes the Peltier effect weakened and the effective temperature difference increases accordingly. Moreover, the results also show the effective temperature difference was raised to 13.6 °C (a 10.2% increase) and the maximum output power was raised to 0.59 W (a 14.8% increase) for the TEG model with fin height of 100 mm (H_{fin5}) compared with that without fins (H_{fin1}) when the output power reaches the maximum value. It should be noted that when the fin height is within a certain range, the performance is obviously improved. But the improvement of the performance will be limited when the value is greater than the threshold value. According to the results above, the output power increased by 8.2% when the H_{fin} increases from 0 mm to 25 mm, but when it increases from 75 mm to 100 mm, the output power only increased by 1.1%. Besides, when the heat transfer conditions of the hot side are weak and the TEG module reaches the maximum output power, the ratio of the load resistance to the internal resistance (r_l/r_i) is larger. The radio increased from 1.14 for H_{fin5} to 1.31 for H_{fin1} due to the more significant Peltier effect.

7. Conclusion

A three-dimensional TEG model is established which consists of 127 pairs of thermocouples. Temperature dependent material properties were considered in the finite-element model, and an experimental TEG system is built up to verify the accuracy of the model. The open circuit voltage, internal resistance and output power have been studied by computational and experimental methods. In summary, the simulation results are in good agreement with the experimental data and the maximum deviation is less than 6%, which proved the accuracy of the present numerical model. Based on this model, the influences of Peltier effect on performances, temperature distribution, and equivalent thermal conductivity have been investigated. The following conclusions were reached: (1) the load resistance and the internal resistance are inconsistent when the output power of TEG reaches the maximum. (2) The heat flow in TEG increased by 30.2% due to the Peltier effects. Consequently, the equivalent thermal conductivity increased by 30.2% due to the increase of heat flow. (3) The influence of Peltier effects on the effective temperature difference is limited when the temperature at the boundary is constant. (4) For convective heat transfer boundaries, the numerical results showed that the effective temperature difference was raised by 13.6 °C (a 10.2% increase) and the maximum output power was raised by 0.59 W (a 14.8% increase) for the TEG model with fin height of 100 mm (H_{fin5}) compared with that without fins (H_{fin1}) when the output power reaches the maximum value. (5) The radio of load resistance to internal resistance increases from 1.14 to 1.34. The results of the model showed that the temperature distributions of TEG module are deeply influenced by the Peltier effect. As a consequence, the influence of the Peltier effect cannot be neglected in the study of heat transfer performance, especially when the heat transfer condition at the hot side is weak or the internal resistance of the TEG module is low.

Acknowledgement

This work is supported by the National Natural Science Foundation of China (51404176, 11402179, 11572274) and the Open Research Fund of Key Laboratory for Ferrous Metallurgy and Resources Utilization of Ministry of Education, Wuhan University of Science and Technology (FMRU201503).

References

[1] H. Kaibe, K. Makino, T. Kajihara, S. Fujimoto, H. Hachiuma, Thermoelectric generating system attached to a carburizing furnace at Komatsu Ltd., Awazu Plant. (2012) 524–527.
[2] M.F. Remeli, A. Date, B. Orr, L.C. Ding, B. Singh, N.D.N. Affandi, et al., Experimental investigation of combined heat recovery and power generation using a heat pipe assisted thermoelectric generator system, Energy Convers. Manage. 111 (2016) 147–157.
[3] F.X. Villasevil, A.M. López, High-efficiency photovoltaic technology including thermoelectric generation, J. Power Sources 252 (2014) 264–269.
[4] X.F. Zheng, C.X. Liu, Y.Y. Yan, Q. Wang, A review of thermoelectrics research – recent developments and potentials for sustainable and renewable energy applications, Renew. Sustain. Energy Rev. 32 (2014) 486–503.

[5] L.G. Chen, F.K. Meng, F.R. Sun, Thermodynamic analyses and optimization for thermoelectric devices: the state of the arts, Sci. China 59 (2016) 442–455.
[6] L. Chen, F. Meng, G.E. Yanlin, F. Sun, Progress in thermodynamic studies for semiconductor thermoelectric devices, J. Mech. Eng. 49 (2013) 144.
[7] L.D. Zhao, S.H. Lo, Y. Zhang, H. Sun, G. Tan, C. Uher, et al., Ultralow thermal conductivity and high thermoelectric figure of merit in SnSe crystals, Nature 508 (2014) 373.
[8] Y. Sun, P. Sheng, C. Di, F. Jiao, W. Xu, D. Qiu, et al., Organic thermoelectric materials and devices based on p- and n-type poly(metal 1,1,2,2-ethenetetrathiolate)s, Adv. Mater. 24 (2012) 932–937.
[9] A. Montecucco, J.R. Buckle, A.R. Knox, Solution to the 1-D unsteady heat conduction equation with internal Joule heat generation for thermoelectric devices, Appl. Therm. Eng. 35 (2012) 177–184.
[10] X.C. Xuan, K.C. Ng, C. Yap, H.T. Chua, A general model for studying effects of interface layers on thermoelectric devices performance, Int. J. Heat Mass Transf. 45 (2002) 5159–5170.
[11] M. Chen, L.A. Rosendahl, T. Condra, A three-dimensional numerical model of thermoelectric generators in fluid power systems, Int. J. Heat Mass Transf. 54 (2011) 345–355.
[12] W.H. Chen, C.Y. Liao, C.I. Hung, A numerical study on the performance of miniature thermoelectric cooler affected by Thomson effect, Appl. Energy 89 (2012) 464–473.
[13] D.N. Kossyvakis, C.G. Vossou, C.G. Provatidis, E.V. Hristoforou, Computational and experimental analysis of a commercially available Seebeck module, Renew. Energy 74 (2015) 1–10.
[14] D. Mitrani, J. Salazar, One-dimensional modeling of TE devices considering temperature-dependent parameters using SPICE, Microelectron. J. 40 (2009) 1398–1405.
[15] E.E. Antonova, D.C. Looman, Finite elements for thermoelectric device analysis in ANSYS (2005) 215–218.
[16] O. Yamashita, Effect of linear and non-linear components in the temperature dependences of thermoelectric properties on the energy conversion efficiency, Energy Convers. Manage. 86 (2009) 1746–1756.
[17] U. Erturun, K. Erermis, K. Mossi, J. Yan, Influence of leg sizing and spacing on power generation and thermal stresses of thermoelectric devices, Appl. Energy 159 (2015) 19–27.
[18] W. Li, J. Peng, W. Xiao, H. Wang, J. Zeng, J. Xie, et al., The temperature distribution and electrical performance of fluid heat exchanger-based thermoelectric generator, Appl. Therm. Eng. 118 (2017) 742–747.
[19] L. Chen, J. Gong, F. Sun, C. Wu, Effect of heat transfer on the performance of thermoelectric generators, Int. J. Therm. Sci. 41 (2002) 95–99.
[20] G.Y. Huang, C.T. Hsu, C.J. Fang, D.J. Yao, Optimization of a waste heat recovery system with thermoelectric generators by three-dimensional thermal resistance analysis, Energy Convers. Manage. 126 (2016) 581–594.
[21] H.S. Dizaji, S. Jafarmadar, S. Khalilarya, A. Moosavi, An exhaustive experimental study of a novel air-water based thermoelectric cooling unit, Appl. Energy 181 (2016) 357–366.
[22] C.H. Cheng, S.Y. Huang, T.C. Cheng, A three-dimensional theoretical model for predicting transient thermal behavior of thermoelectric coolers, Int. J. Heat Mass Transf. 53 (2010) 2001–2011.
[23] C.H. Cheng, S.Y. Huang, Development of a non-uniform-current model for predicting transient thermal behavior of thermoelectric coolers, Appl. Energy 100 (2012) 326–335.
[24] D.M. Rowe, Thermoelectrics Handbook: Macro to Nano, 2005.
[25] H.J. Goldsmid, Theory of Thermoelectric Refrigeration and Generation, Springer Berlin Heidelberg, 2010.
[26] C. Jiang, X.A. Fan, Z. Rong, C. Zhang, G. Li, B. Feng, et al., Elemental diffusion and service performance of Bi_2Te_3-based thermoelectric generation modules with flexible connection electrodes, J. Electron. Mater. 1–8 (2016).
[27] J.Y. Jang, Y.C. Tsai, Optimization of thermoelectric generator module spacing and spreader thickness used in a waste heat recovery system, Appl. Therm. Eng. 51 (2013) 677–689.
[28] N.S. Benday, D.M. Dryden, K. Kornbluth, P. Stroeve, A temperature-variant method for performance modeling and economic analysis of thermoelectric generators: linking material properties to real-world conditions, Appl. Energy 190 (2017) 764–771.
[29] J.H. Meng, X.D. Wang, X.X. Zhang, Transient modeling and dynamic characteristics of thermoelectric cooler, Appl. Energy 108 (2013) 340–348.